Response and instability prediction of helicopter dynamics on the ground

Leonardo Sanches, Guilhem Michon, Alain Berlioz, Daniel Alazard

Response and instability prediction of helicopter dynamics on the ground

L. Sanches [a,*], G. Michon [b], A. Berlioz [c], D. Alazard [d]

[a] Universidade Federal de Uberlândia, Faculdade de Engenharia Mecânica, Laboratório de Mecânica de Estruturas Prof. José Eduardo Tannús Reis, Brazil
[b] Université Toulouse, ICA, ISAE, France
[c] Université Toulouse, ICA, UPS, France
[d] Université Toulouse, DMIA, ISAE, France

In helicopters with hinged blades an unstable dynamical phenomenon known as ground resonance may occur during take-off and landing and lead to the total destruction of the aircraft. Predicting the phenomenon is necessary to determine the stability of periodical equations of motion. The instability boundaries can be easily obtained for isotropic rotor configurations through multi-blade coordinate transformation once the periodic terms are eliminated. However, Floquet's theory is commonly used to treat the periodic motion equations when introducing the asymmetric effects of spring or damper aging or rotor rupture (anisotropic rotors). In additional, it is known that when treated as parametric excitations, periodic terms may lead to instability in dynamical systems under parametric resonances. In this paper a helicopter in contact with the ground is considered as a parametrically excited system and the equations are treated analytically by applying the method of multiple scales (MMS). A stability analysis verifies the existence of parametric instabilities by first order sets of equations for an isotropic rotor configuration. The results are compared and validated with those obtained by using Floquet's Theory. Moreover, the amplitude responses of the aircraft at equilibrium in the remaining resonant cases are studied. The results are then compared with those obtained from the time response analysis.

1. Introduction

An unstable phenomenon in helicopter dynamics known as ground resonance consists of a self-excited oscillation caused by the interaction between rotor blade oscillations and other forms of movement in the helicopter [1]. Several accidents have been recorded that have shown that, under certain conditions, the phenomenon can be very violent and lead to the total destruction of the aircraft.

The earliest research into the phenomenon was performed by Coleman and Feingold [2] who laid the foundations for all subsequent studies into the problem. Donham et al. [3] and Lytwyn et al. [4] added the air resonance effect and verified its influence on the phenomenon. Major contributions towards understanding the phenomenon of ground resonance in hingeless and bearingless rotors were made by army researchers, such as Hodges [5]. Recently, Kunz [6] analyzed the influence of non-linear springs and dampers (elastomeric elements) for predicting the rotor instability zone while Byers and Gandhi [7] explored how the problem might be controlled passively.

The investigations mentioned above demonstrated that the occurrences of ground resonance can be accurately predicted for articulated, hingeless and bearingless rotors. The use of linearized equations of motion provides very accurate frequency prediction.

These works all focused on analyzing isotropic rotor configurations (all blades having the same properties). The boundary speeds of ground resonance are easily obtained once the periodic terms are eliminated through a variable transformation known as the Coleman Transformation or, more generally, as the multi-blade coordinate transformation [8].

Nevertheless, the case of anisotropic rotors is very interesting from the practical point of view. Indeed, due to aging, damper and stiffness properties can change from one blade to another. Consequently, as the Coleman Transformation can no longer be applied to such anisotropic rotors, the periodical equations of motion are subjected to a stability analysis.

In a recent study on helicopter dynamics, and more specifically on the ground resonance phenomenon, Sanches et al. [9], retained the periodic terms in the equations of motion. Using Floquet's Method the instability zones predicted were similar to those Coleman and Feingold predicted for an isotropic rotor.

* Corresponding author.
E-mail address: lsanches@femec.ufu.br (L. Sanches).

Nomenclature

Symbol	description, units
a	rotor eccentricity, m
b	blade center of giration, m
[c.c]	complex conjugate terms
D_n^p	$\partial^p / \partial T_n^p$ – partial derivative with respect to time scales
$\mathbf{F}_{\text{ext}}$	external force vector
$\mathbf{G}$	damping matrix of the dynamical system
i	complex number
I_{Zbk}	lag rotational inertia of the kth blade around its center of gravity, kg m^2
$\mathbf{K}$	stiffness matrix of the dynamical system
K_{bk}	kth blade lead-lag stiffness, N m rad^{-1}
K_{f_x}, K_{f_Y}	longitudinal and transversal stiffness of fuselage, N m^{-1}
m_f, m_{bk}	fuselage and mass of kth blade, kg
$\mathbf{M}$	mass matrix of the dynamical system
N_b	number of blades in the rotor
$P(\Gamma, \sigma)$	characteristic polynomial equation of 4th degree in
r_{ak}	$\sqrt{ar_{bk}}$
r_{bk}	ratio between the static moment over the total lead-lag rotational inertia of the kth blade, m^{-1}
r_{mk}	ratio between the static moment of the kth blade over the total mass of the helicopter, m
$\mathbf{S}$	state space matrix
t	time, s
T_0, T_1	time scales, s
$\mathbf{u}$	general variables
$\mathbf{V}$	state variables
$x(t)$, $y(t)$	longitudinal and transversal displacement of the fuselage, m
x_{bx}, y_{bx}	blade position in x and y directions, m
(x, y, z)	mobile coordinate system attached to the rotor hub
(X_0, Y_0, Z_0)	inertial referential system

Greek Letters

α, β	given by the relation in
ϵ	bookkeeping parameter
$\varphi_k(t)$	lead–lag angle of kth blade, rad
$\mathbf{\Phi}$	transition matrix (Floquet's Theory)
Γ	solutions of the characteristic polynomial equation
λ	characteristic exponents
Ω	rotor speed, rad s^{-1}
σ	frequency detuning parameter, rad s^{-1}
ζ_k	azimuth angle for the kth blade, rad
$\omega_{1\ldots6}$	the six general natural frequencies of Eq. (14), rad s^{-1}
ω_{bk}	lag resonance frequency of the kth blade at, rad s^{-1}
ω_x, ω_y	fuselage resonance frequencies in x and y directions, rad s^{-1}

In previous studies the anisotropic rotor was treated by using Floquet's Theory [10,11]. Since the stability analysis is performed through the monodromy matrix and calculated for each combination of input parameters, the current method is expensive in terms of computer time.

Analytical mathematical methods have already been developed and dedicated to calculating differential equations with periodical coefficients. Moreover, once the analytical responses are determined, the boundaries of instabilities can easily be obtained for any type of rotor configuration. Among these methods mention can be made of [12,13]: Hill's Infinite Determinant, Harmonic Balance Method and Method of Multiple Scales.

The latter method has been frequently applied to periodic, parametric and non-linear problems in industry [14] and in rotating dynamic systems [15–17].

Classic examples of parametrically excited systems (i.e., pendulum dynamics over a parametrically excited base and the oscillatory motion of a string under harmonic axial forces) show that the system is dynamically unstable under parametrical resonance conditions [18].

The present work therefore considers the system as a parametrically excited system and treats it by using the Method of Multiple Scales. The boundaries of the ground resonance phenomenon are obtained by a stability analysis for an isotropic rotor configuration. The results are compared with those obtained by using Floquet's Theory. Then, analysis of the amplitude response of the helicopter is carried out on the remaining parametric resonances.

In Section 2, the dynamical equations of motion from the mechanical model are formulated by neglecting the aerodynamic forces and no viscous damping is taking into account. In Sections 3 and 4, the methodologies applied to the set of periodic motion equations, i.e. the Floquet's Method (FM) and the Method of Multiple Scales (MMS), are described. In Section 5, the critical rotor speeds predicted by both methods are presented and compared for an isotropic rotor configuration. A description is also given of the development of the amplitude responses analysis and the results, while Section 6 presents the conclusions.

2. Mechanical model

The mechanical model used is similar to that proposed by Coleman and Feingold and is developed to characterize the dynamical behavior of a helicopter with a hinged rotor. In other words, it consists of figuring out the relation between the longitudinal and lateral displacement – $x(t)$ and $y(t)$ – of the fuselage and the kth blade lag angle – $\varphi(t)$ – in terms of rotor speed Ω and time t. Fig. 1 provides a general diagram of the system.

The fuselage is considered as a rigid body with its center of gravity at point O. At the outset or initial time, the origin of an inertial coordinate system (X_0, Y_0, Z_0) is coincident at this point. The body is connected to springs that represent the flexibility of the landing skid. The rotor head system consists of an assembly of one rigid rotor hub with Nb blades. Each blade is represented by a damped mass located at a distance b from the lag articulation

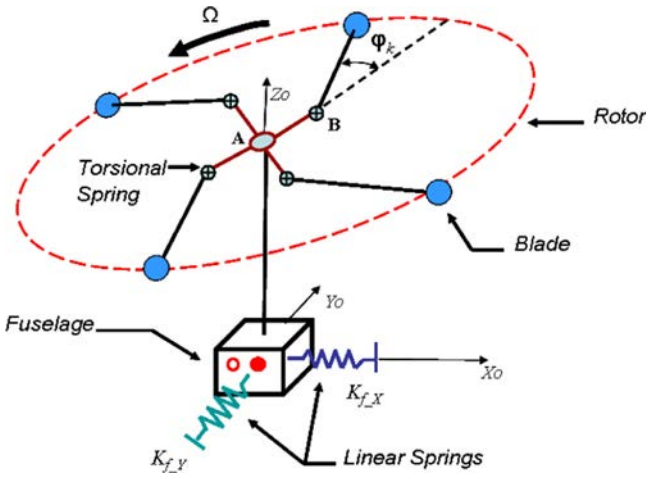

Fig. 1. Diagram of the mechanical system.

(point B) and a torsional spring is linked to each articulation. The origin of a mobile coordinate system (x, y, z) parallel to the inertial one is located at the geometric center of the rotor hub (point A). Both body and rotor head are joined by a rigid shaft, but no aerodynamic forces on the blades and no viscous damping are taken into account.

$$\mathbf{M}(t)=\begin{bmatrix} 1 & 0 & -r_{m1}\sin(\psi_1) & -r_{m2}\sin(\psi_2) & -r_{m3}\sin(\psi_3) & -r_{m4}\sin(\psi_4) \\ 0 & 1 & r_{m1}\cos(\psi_1) & r_{m2}\cos(\psi_2) & r_{m3}\cos(\psi_3) & r_{m4}\cos(\psi_4) \\ -r_{b1}\sin(\psi_1) & r_{b1}\cos(\psi_1) & 1 & 0 & 0 & 0 \\ -r_{b2}\sin(\psi_2) & r_{b2}\cos(\psi_2) & 0 & 1 & 0 & 0 \\ -r_{b3}\sin(\psi_3) & r_{b3}\cos(\psi_3) & 0 & 0 & 1 & 0 \\ -r_{b4}\sin(\psi_4) & r_{b4}\cos(\psi_4) & 0 & 0 & 0 & 1 \end{bmatrix} \tag{2}$$

$$\mathbf{G}(t)=\begin{bmatrix} 0 & 0 & -2\Omega r_{m1}\cos(\psi_1) & -2\Omega r_{m2}\cos(\psi_2) & -2\Omega r_{m3}\cos(\psi_3) & -2\Omega r_{m4}\cos(\psi_4) \\ 0 & 0 & -2\Omega r_{m1}\sin(\psi_1) & -2\Omega r_{m2}\sin(\psi_2) & -2\Omega r_{m3}\sin(\psi_3) & -2\Omega r_{m4}\sin(\psi_4) \\ 0 & 0 & 0 & 0 & 0 & 0 \\ 0 & 0 & 0 & 0 & 0 & 0 \\ 0 & 0 & 0 & 0 & 0 & 0 \\ 0 & 0 & 0 & 0 & 0 & 0 \end{bmatrix} \tag{3}$$

$$\mathbf{K}(t)=\begin{bmatrix} \omega_x^2 & 0 & \Omega^2 r_{m1}\sin(\psi_1) & \Omega^2 r_{m2}\sin(\psi_2) & \Omega^2 r_{m3}\sin(\psi_3) & \Omega^2 r_{m4}\sin(\psi_4) \\ 0 & \omega_y^2 & -\Omega^2 r_{m1}\cos(\psi_1) & -\Omega^2 r_{m2}\cos(\psi_2) & -\Omega^2 r_{m3}\cos(\psi_3) & -\Omega^2 r_{m4}\cos(\psi_4) \\ 0 & 0 & \omega_{b1}^2+\Omega^2 r_{a1}^2 & 0 & 0 & 0 \\ 0 & 0 & 0 & \omega_{b2}^2+\Omega^2 r_{a2}^2 & 0 & 0 \\ 0 & 0 & 0 & 0 & \omega_{b3}^2+\Omega^2 r_{a3}^2 & 0 \\ 0 & 0 & 0 & 0 & 0 & \omega_{b4}^2+\Omega^2 r_{a4}^2 \end{bmatrix} \tag{4}$$

2.1. Equations of motion

The equations of motion are obtained by introducing a Lagrange equation in the kinetic and potential energy expressions of the system (body and rotor). To achieve this goal, the following conditions are considered:

1. The fuselage has a mass m_f and the spring stiffness linked to it K_{fX} and K_{fY} through x and y directions, respectively.
2. The rotor is composed of $N_b=4$ blades and each blade k has an azimuth angle of $\zeta_k=2\pi(k-1)/N_b$ with the x-axis.
3. Each blade has the same mass m_{bk} and moment of inertia I_{zbk} around the z-axis.
4. The angular spring constant for each k blade is K_{bk}.
5. The position of blade k projected in the inertial coordinate system is

$$x_{bk}=a\cos(\Omega t+\zeta_k)+b\cos(\Omega t+\zeta_k+\varphi_k(t))+x(t)$$
$$y_{bk}=a\sin(\Omega t+\zeta_k)+b\sin(\Omega t+\zeta_k+\varphi_k(t))+y(t)$$

where a is the hinge offset.

Considering the general Laplace variable $\mathbf{u}$ as

$$\mathbf{u}_{1\ldots6}(t)=\{x(t)\ y(t)\ \varphi_1(t)\ \varphi_2(t)\ \varphi_3(t)\ \varphi_4(t)\}$$

we obtain the vector of degrees of freedom of the system.

The linear matrix equation of motion of the dynamical system, represented in Eq. (1), is obtained by neglecting the non-linear terms and performing a first order Taylor series expansion for the trigonometric blade lead–lag angle terms.

$$\mathbf{M}\ddot{\mathbf{u}}+\mathbf{G}\dot{\mathbf{u}}+\mathbf{K}\mathbf{u}=\mathbf{F_{ext}} \tag{1}$$

$\mathbf{M}$, $\mathbf{G}$ and $\mathbf{K}$ correspond to the mass, damping and stiffness matrix, respectively. They are non-symmetric and non-diagonal matrices due to the presence of periodic terms. Moreover, $\mathbf{F_{ext}}$ is equal to zero for blades with same inertial and geometrical properties. They are all expressed in Eqs. (2)–(5), in the following:

$$\mathbf{F_{ext}}(t)=\begin{bmatrix} \sum_{k=1}^{N_b}\Omega^2 r_{mk}\left(\frac{a+b}{a}\right)\cos(\psi_k) \\ \sum_{k=1}^{N_b}\Omega^2 r_{mk}\left(\frac{a+b}{a}\right)\sin(\psi_k) \\ 0 \\ 0 \\ 0 \\ 0 \end{bmatrix} \tag{5}$$

where

$$r_{mk}=\frac{bm_{bk}}{m_f+\sum_{k=1}^{N_b}m_{bk}},\quad r_{bk}=\frac{bm_{bk}}{b^2m_{bk}+I_{z_{bk}}},$$
$$r_{ak}^2=ar_{bk},\quad \psi_k=\Omega t+\zeta_k,$$
$$\omega_x^2=\frac{K_{fX}}{m_f+\sum_{k=1}^{N_b}m_{bk}},\quad \omega_y^2=\frac{K_{fY}}{m_f+\sum_{k=1}^{N_b}m_{bk}},$$
$$\omega_{bk}^2=\frac{K_{bk}}{b^2m_{bk}+I_{z_{bk}}},\quad k=1\ldots N_b$$

It should be noted that factors r_{mk} and r_{bk}, which represent the ratio between the blade static moment over the helicopter's total translatory inertia of the helicopter and the blade's total rotational inertia of the blade, respectively, are smaller when compared to the unit.

The terms ω_x and ω_y are the resonance frequencies of the fuselage in directions x and y, respectively. Moreover, $\omega_{b3\ldots6}$ are the lead–lag resonance frequencies of blades 1–4.

3. Floquet's method

In this section, a stability analysis of the periodic equations of motion is conducted by using Floquet's theory for predetermining the critical speeds of the rotor that can lead to ground resonance [11]. By representing the dynamical system in a state-space format and considering the state-space matrix $\mathbf{S}(t)$ with period T of Eq. (1), the system becomes

$$\dot{\mathbf{v}}(t)=\mathbf{S}(t)\mathbf{v}(t), \quad t>t_0$$
$$\mathbf{v}(t)=\mathbf{v}_0, \quad \mathbf{v}(t)=[\mathbf{u}(t)\ \ \dot{\mathbf{u}}(t)]^T$$

where $\mathbf{v}(t)$ is the state variable.

According to Floquet's Theory, a transition matrix $\mathbf{\Phi}$, which relates $\mathbf{v}(t_0)$ to $\mathbf{v}(t)$, is defined as $\mathbf{\Phi}(t,t_0)=\mathbf{P}(t,t_0)\exp((t-t_0)\mathbf{Q})$.

The monodromy matrix **R,** defined as

$$\mathbf{R}=\mathbf{\Phi}(t_0+T,\ t_0)$$

is computed by admitting the periodic system matrices – Eq. (1) – as a switched periodical system. As reported by Dufour and Berlioz [19], the matrix $\mathbf{S}(t)$ is approximated by a series of p step functions and the monodromy matrix can be obtained as

$$\mathbf{R}=\prod_{k=1}^{p} e^{\mathbf{S}_k(t_k-t_{k-1})} \tag{6}$$

where matrix $\mathbf{S}_k$, within the interval defined by t_k and t_{k-1}, is a constant value of $\mathbf{S}(t)$ at $t=t_{k-1}$.

The matrix $\mathbf{Q}$ can be obtained through the following relation:

$$\mathbf{Q}=\frac{1}{T}\log(\mathbf{R})$$

The dynamical system Eq. (1) is stable if the eigenvalues (λ) of $\mathbf{Q}$, also called characteristic exponents, are negative. Similarly, the system is stable if all the norms of the eigenvalues of $\mathbf{R}$, known as characteristic multipliers, are less than one.

4. Method of multiple scales

Asymptotic methods are often used to obtain analytical solutions for non-linear and periodic equations. The Method of Multiple Scales – MMS [13,12] is then used to treat the periodical equations of movement.

By introducing the bookkeeping parameter, all the time dependent functions are expressed as a function of multiple scales of time and represented by an expansion having the form:

$$\mathbf{u}_n(t)=\mathbf{u}_{n_0}(T_0,T_1)+\epsilon\mathbf{u}_{n_1}(T_0,T_1)+\mathcal{O}(2), \quad n=1\ldots6 \tag{7}$$

where $T_n=\epsilon^n t$, $n\in\mathbb{R}+$.

By substituting Eq. (7) in Eq. (1) and considering $r_{mk}=\epsilon\alpha_k$ and $r_{bk}=\epsilon\beta_k$, two sets of equations are obtained by grouping them as a function of the power of ϵ. Terms with an order higher than ϵ^2 are neglected. The periodic terms are considered as parametric excitations and scaled to appear at the order of ϵ.

4.1. Order ϵ^0 equations

The set of order ϵ^0 equations of the system is collected. They represent the steady-state response of the uncoupled rotor and fuselage dynamical system.

$$D_0^2u_{n_0}(T_0,T_1)+\omega_n^2u_{n_0}(T_0,T_1)=0, \quad n=1\ldots6 \tag{8}$$

where D_0 is the partial derivative as a function of T_0 and

$$\omega_1=\omega_x,\omega_2=\omega_y,\omega_{k+2}=\sqrt{\omega_{bk}^2+r_{ak}^2\Omega^2}, \quad k=1\ldots N_b$$

The solutions of these homogeneous equations are trivial and take the form $u_{n_0}=\frac{1}{2}\ C_n(T_1)e^{(i\omega_nT_0)}+[c.c]$, $n=1\ldots6$. Term $C_n(T_1)$ is complex and [c.c] represents the complex conjugate of the previous terms.

4.2. Order ϵ^1 equations

In the following, Eqs. (9)–(12) represent the set of equations of order ϵ^1.

$$\begin{aligned}&D_0^2u_{1_1}(T_0,T_1)+\omega_1^2u_{1_1}(T_0,T_1)=-2D_1D_0u_{1_0}(T_0,T_1)\\&+\sum_{n=3}^{6}\left\{\begin{array}{c}-\frac{1}{2}i^{(n-2)}\alpha_{n-2}D_0^2u_{n_0}(T_0,T_1)e^{(i\Omega T_0)}\\+i^{(n-3)}\alpha_{n-2}\Omega D_0u_{n_0}(T_0,T_1)e^{(i\Omega T_0)}\\+\frac{1}{2}i^{(n-2)}\alpha_{n-2}\Omega^2u_{n_0}(T_0,T_1)e^{(i\Omega T_0)}+[c.c]\end{array}\right\}\end{aligned} \tag{9}$$

$$\begin{aligned}&D_0^2u_{2_1}(T_0,T_1)+\omega_2^2u_{2_1}(T_0,T_1)=-2D_1D_0u_{2_0}(T_0,T_1)\\&+\sum_{n=3}^{6}\left\{\begin{array}{c}-\frac{1}{2}i^{(n-3)}\alpha_{n-2}D_0^2u_{n_0}(T_0,T_1)e^{(i\Omega T_0)}\\-i^{(n-2)}\alpha_{n-2}\Omega D_0u_{n_0}(T_0,T_1)e^{(i\Omega T_0)}\\+\frac{1}{2}i^{(n-3)}\alpha_{n-2}\Omega^2u_{n_0}(T_0,T_1)e^{(i\Omega T_0)}+[c.c]\end{array}\right\}\end{aligned} \tag{10}$$

$$\begin{aligned}&D_0^2u_{n_1}(T_0,T_1)+\omega_n^2u_{n_1}(T_0,T_1)\\&=-2D_1D_0u_{n_0}(T_0,T_1)+-\frac{1}{2}i^{(n-2)}\beta_{n-2}D_0^2u_{1_0}(T_0,T_1)e^{(i\Omega T_0)}\\&\quad-\frac{1}{2}i^{(n-3)}\beta_{n-2}D_0^2u_{2_0}(T_0,T_1)e^{(i\Omega T_0)}+[c.c], \quad n=3\ldots6\end{aligned} \tag{11}$$

As can be observed, the excitation terms (i.e. the right-hand side of the above equations) are totally dependent on the steady-state responses u_{n_0}.

4.2.1. Parametric resonances of first order – ϵ^1 equations

By substituting the solutions of Eq. (8) in Eq. (9) to Eq. (11), the product $u_{n_0}(T_0,T_1)e^{(i\Omega T_0)}$ and its conjugate term are represented as $C_n(T_1)e^{i(\Omega\pm\omega_n)T_0}+[cc]$. The exponents, expressed as a function of ω_n and Ω, are harmonics of the excitation terms. Depending on their origin (fuselage or blade equations), the different types of harmonics found are presented in the following:

Body Eqs. (9) and (10):

$$[\|\Omega\pm\omega_n\|], \quad n=3\ldots6 \tag{12}$$

Blade Eq. (11):

$$[\|\Omega\pm\omega_1\| \ \ \|\Omega\pm\omega_2\|] \tag{13}$$

Depending on the rotor speed value attributed for Ω, when a harmonic is identical to the natural frequencies ($\omega_{1\ldots6}$), a resonance condition is identified on the equations of ϵ^1 order. Under this condition, the corresponding term is considered as a secular term [12] and the resonance is denominated as a parametric resonance of the first order.

The possible critical rotor speeds at which a resonance occurs are

Body equation – Eq. (9):

$$[\|\omega_1\pm\omega_3\| \ \ \|\omega_1\pm\omega_4\| \ \ \|\omega_1\pm\omega_5\| \ \ \|\omega_1\pm\omega_6\|] \tag{14}$$

Body equation – Eq. (10):

$$[\|\omega_2\pm\omega_3\| \ \ \|\omega_2\pm\omega_4\| \ \ \|\omega_2\pm\omega_5\| \ \ \|\omega_2\pm\omega_6\|] \tag{15}$$

Blade Eq. (11):

$$[\|\omega_1\pm\omega_n\| \ \ \|\omega_2\pm\omega_n\|], \quad n=3\ldots6 \tag{16}$$

They are calculated by solving Eq. (12) equal to ω_1 and ω_2 and Eq. (13) equal to $\omega_{3\ldots6}$, respectively.

4.2.2. Solvability conditions – ϵ^1 equations

Certain conditions, usually known as solvability or compatibility conditions, must be satisfied when using perturbation methods so that the inhomogeneous equations possess solutions. With MMS, the secular terms should be eliminated by setting their

coefficients equal to zero. A set of equations known as solvability equations are then obtained.

Analysis of the solvability equations enables substantial information concerning the dynamical system to be extracted. This makes it possible to consider predicting the ground resonance phenomenon, by identifying the boundary speeds of unstable zones and studying the amplitude responses as a function of rotor speed (only for stable resonant cases).

Consequently, a detuning frequency parameter σ is introduced only in the harmonic terms before scaling the equations of motion in Eq. (1) by considering $\Omega = \Omega_R + \epsilon\sigma$. This enables the proximity of a resonance case identified by Ω_R and listed in Eqs. (14)–(16) to be controlled.

5. Case study – isotropic rotor

Table 1 contains the data used in the numerical analysis of a helicopter with an isotropic rotor. Firstly, a stability analysis is carried out at each parametric resonance case and the boundaries of the unstable regions determined. However, if stable oscillations are found, then the amplitude responses of the helicopter at equilibrium are studied. The results will be compared later with those obtained by a step-by-step numerical integration.

5.1. Stability analysis

Both FM and MMS methods are used to predict the boundary speeds of the ground resonance phenomenon. The results obtained by MMS, in which the helicopter is considered as a parametrically exited system, are also compared with those found by FM.

Fig. 2 shows the evolution of the multiplier characteristic along with the rotor speed obtained from FM by considering the period divided in $p=64$ parts. The unstable regions, delineated by strictly absolute values of the ordinate greater than one, are given in Table 3.

Nevertheless, parametric resonances are verified with MMS, as mentioned in Sections 4.2.1 and 4.2.2. The critical rotor values are illustrated graphically in Fig. 3 which shows the evolution of the natural frequencies (ω_1–ω_6) with the evolution of the harmonics of exciting terms (see Eq. (12)) as a function of rotor speed Ω. Four resonance cases (A, B, C and D) are observed and it should be noted that two resonances occur simultaneously for each one. Table 2 gives the rotor speed values for all cases.

Table 1
Numerical values of the fuselage and rotor head inputs.

Fuselage		Rotor		
$m_f = 2902.9$		$m_{bk} = 31.9$	$a = 0.2$	$b = 2.5$
$\omega_x = 6.0\pi$	$\omega_y = 8.0\pi$	$\omega_y = 3.0\pi$	$I_{zb} = 259$	

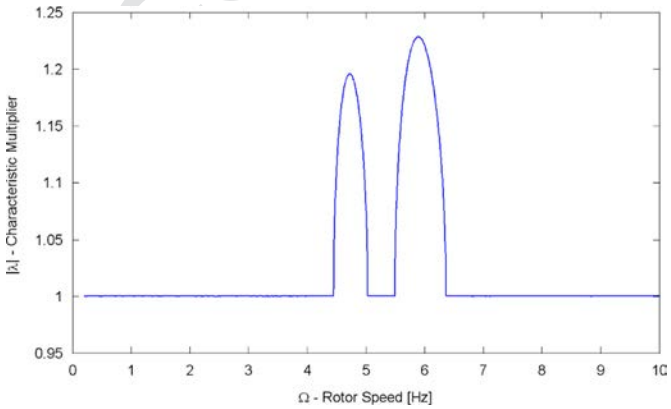

Fig. 2. Evolution of the exponent characteristics for an isotropic rotor configuration.

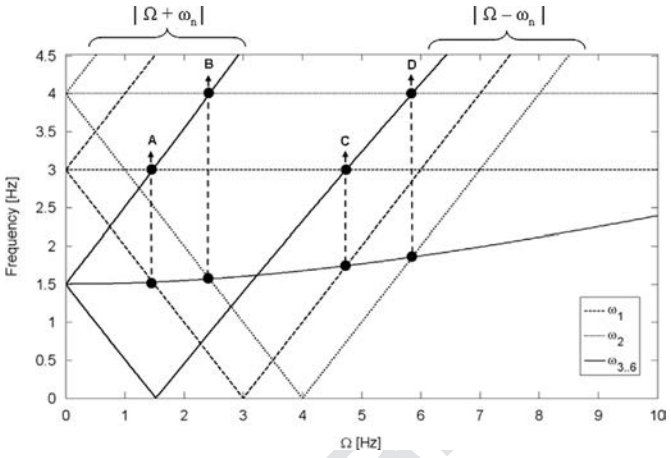

Fig. 3. Evolution of harmonic combinations with the evolution of natural frequencies for an isotropic rotor at ϵ^1 equations.

Table 2
Rotor speed values in Hz of the parametric resonance cases identified by MMS for an isotropic rotor.

Resonant cases of first order			
A	B	C	D
1.475	2.433	4.743	5.857

5.1.1. Stability analysis – ϵ^1 equations

At each resonance case the solvability equations undergo a stability study and the boundaries of instability are determined. Since the blades have the same geometrical and inertial properties and assuming $\epsilon = r_m$, we obtain $\alpha_k = \alpha = 1$ and $\beta_k = \beta = r_{bk}/r_{mk}$ for $k=1\ldots4$.

- Case A - $\Omega_R = \omega_1 - \omega_{3\ldots6} = 1.475*(2\pi)$

The solvability equations are presented below:

$$-2i\left(\frac{\partial}{\partial T_1}C_1\right)\omega_1 + \sum_{n=3}^{6} i^{(n-2)}\alpha\left(\frac{1}{2}\omega_n^2\, e^{i\sigma T_1} + \Omega_R\,\omega_n e^{i\sigma T_1} + \frac{1}{2}\Omega_R^2 e^{i\sigma T_1}\right)C_n = 0 \tag{17}$$

$$2i\left(\frac{\partial}{\partial T_1}C_2\right)\omega_2 = 0 \tag{18}$$

$$-2i\left(\frac{\partial}{\partial T_1}C_n\right)\omega_n - \frac{1}{2}i^{(4-n)}\beta C_1\omega_1^2 e^{-i\sigma T_1} = 0, \quad n = 3\ldots6 \tag{19}$$

The above equations become autonomous by substituting the following Cartesian form in the amplitudes C.

$$C_k = (B_{rk} + iB_{ik})e^{(1/2i\sigma T_1)}, \quad k = 1\ldots2$$
$$C_k = (B_{rk} + iB_{ik})e^{(-1/2i\sigma T_1)}, \quad k = 3\ldots6$$

where B_{rk} and B_{ik} are real functions of T_1.

Twelve new expressions are obtained by collecting and separating the real and imaginary terms. They admit nontrivial solutions having the form $[B_{rk},\ B_{ik}] = [d_{rk}, d_{ik}]e^{(\Gamma T_1)}$ where Γ, d_{rk} and d_{ik} are constants.

After arranging the set of equations in matrix form, the polynomial characteristic equation $P_A(\Gamma, \sigma)$, expressed as function

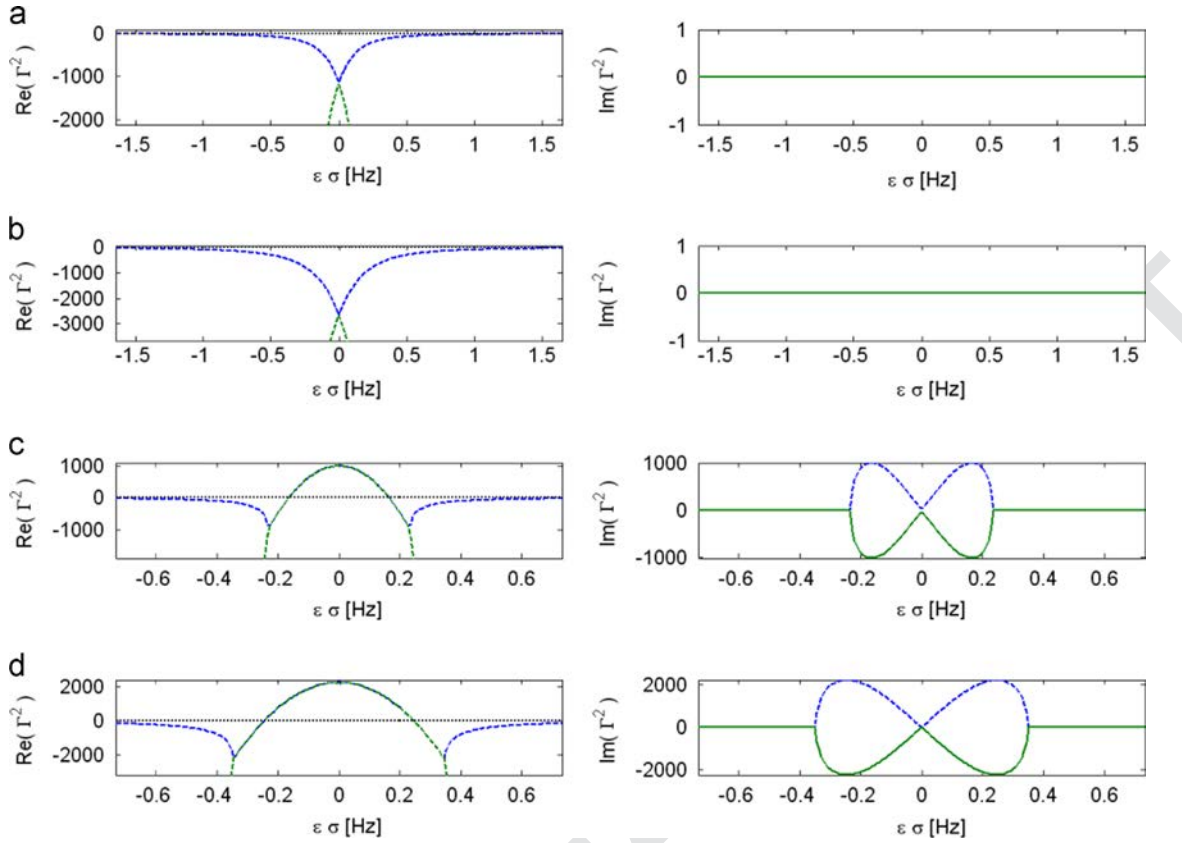

Fig. 4. Stability analysis of the first order resonance Cases A, B, C and D. (1) Evolution of the real part of Γ^2. (2) Evolution of the imaginary part of Γ^2.

of Γ and σ, is

$$P_A(\Gamma,\sigma)=\Gamma^{12}+a_{10}\Gamma^{10}+a_8\Gamma^8+a_6\Gamma^6+a_4\Gamma^4+a_2\Gamma^2+a_0 \quad (20)$$

where

$$a_0=0.000244140\sigma^{12}+0.00156162\sigma^{10}+0.00249716\sigma^8$$

$$a_2=0.00585936\sigma^{10}+0.0312323\sigma^8+0.0399546\sigma^6$$

$$a_4=0.0585937\sigma^8+0.249858\sigma^6+0.239728\sigma^4$$

$$a_6=0.639272+0.937500\sigma^4+1.99886\sigma^2$$

$$a_8=0.639272+0.937500\sigma^4+1.99886\sigma^2$$

$$a_{10}=1.59909+1.50000\sigma^2$$

The procedure developed previously leads to the polynomial characteristic equation for the remainder of the resonance cases $P_k(\Gamma,\sigma)$, $k=\{A, B, C, D\}$ and their stability is determined by considering the roots (Γ).

The system is stable when, by varying σ over a certain range, the values of Γ are all imaginary. It implies that Γ^2 should be real and negatives. Fig. 4 illustrates the evolution of the real and imaginary values of Γ^2 separately.

Regarding cases A and B, Γ^2 presents purely real and negative values as a function of the product $\epsilon\sigma$ whose value is considered to vary from -0.73 to 0.73 Hz. However, in cases C and D, unstable movements occur when $\epsilon\sigma$ vary from -0.2343 to 0.2343 Hz for case C and from -0.3514 to 0.3514 Hz for case D. The boundaries of instability found by MMS are grouped with those obtained by FM in Table 3. Moreover, the percentual error is presented by comparing the mean rotor speed value of each instability region obtained with both methods.

Table 3
Limits of instability zones predicted by using FM and MMS and the error between the mean rotor speed value by comparing both methods.

Zone/case	With FM		With MMS		Error (%)
1/C	4.446	5.034	4.508	4.978	1.26
2/D	5.495	6.367	5.506	6.208	1.35

5.2. Amplitude response analysis

The amplitude response of the helicopter on stable resonance cases (i.e., A and B) is studied. It consists in deducing the relation between the amplitudes and phases of the fuselage and blade movements and the detuning parameter σ, once equilibrium is reached.

5.2.1. Resonance case A

A polar coordinate transformation defined below is applied to the solvability Eqs. (17)–(19).

$$C_n(T_1)=A_n(T_1)e^{i\theta_n(T_1)}, \quad n=1\ldots6 \quad (21)$$

Two new sets of equations are obtained by separating the real and imaginary terms into groups.

The set of equations composed of real terms is

$$\frac{d}{dT_1}A_1 = 4.71239\,A_3\,\cos(\gamma_1)-4.71239\,A_4\,\sin(\gamma_2) -4.71239\,A_5\,\cos(\gamma_3)+4.71239\,A_6\,\sin(\gamma_4)$$

$$\frac{d}{dT_1}A_2=0$$

$$\frac{d}{dT_1}A_3=-61.3238\,A_1\,\cos(\gamma_1)$$

$$\frac{d}{dT_1}A_4 = 61.3238\, A_1\ \sin(\gamma_2)$$
$$\frac{d}{dT_1}A_5 = 61.3238\, A_1\ \cos(\gamma_3)$$
$$\frac{d}{dT_1}A_6 = -61.3238\, A_1\ \sin(\gamma_4) \tag{22}$$

and the set of equations composed of imaginary terms is

$$\frac{d}{dT_1}\theta_1 = \frac{1}{A_1}\begin{bmatrix} 4.71239\, A_3\ \sin(\gamma_1) + 4.71239\, A_4\ \cos(\gamma_2) \\ -4.71239\, A_5\ \sin(\gamma_3) - 4.71239\, A_6\ \cos(\gamma_4) \end{bmatrix}$$
$$\frac{d}{dT_1}\theta_2 = 0$$
$$\frac{d}{dT_1}\theta_3 = 61.3238\,\frac{A_1\ \sin(\gamma_1)}{A_3}$$
$$\frac{d}{dT_1}\theta_4 = 61.3238\,\frac{A_1\ \cos(\gamma_2)}{A_4}$$
$$\frac{d}{dT_1}\theta_5 = -61.3238\,\frac{A_1\ \sin(\gamma_3)}{A_5}$$
$$\frac{d}{dT_1}\theta_6 = -61.3238\,\frac{A_1\ \cos(\gamma_4)}{A_6} \tag{23}$$

where

$$\gamma_n(T_1) = -\theta_1(T_1) + \sigma T_1 + \theta_{n+2}(T_1), \quad n = 1\ldots4 \tag{24}$$

It should be noted that γ_n are functions of T_1 and express the phase shift between the kth blade lead–lag oscillations and the longitudinal movement of the fuselage. Moreover, the non-existence of any harmonic terms equal to ω_2 explains why the second expression of each set of equations is independent and equal to zero.

Imposing the dynamic system in equilibrium

$$\frac{d}{dT_1}\gamma_n = \frac{d}{dT_1}A_k = 0, \quad n = 1\ldots4,\ \ k = 1\ldots6$$

the values of each γ_n is determined from Eq. (22) by assuming $A_1(T_1)$ and $A_{3\ldots6}(T_1)$ non-nulls.

We verify that two solutions are found in the interval of $]0, 2\pi[$ for each γ and they are represented below as

$$\gamma_1(T_1) = \left\{\frac{\pi}{2}, \frac{3\pi}{2}\right\}$$
$$\gamma_2(T_1) = \{0, \pi\}$$
$$\gamma_3(T_1) = \left\{\frac{\pi}{2}, \frac{3\pi}{2}\right\}$$
$$\gamma_4(T_1) = \{0, \pi\} \tag{25}$$

By combining the possible values of γ, 16 sets of solutions are obtained. The relation between amplitudes A_k and the detuning parameter σ is found for each set, from Eqs. (23) and (24). Likewise, the correlation of the phases θ_k is also acquired.

For instance, by considering the solution set $\gamma_1 = \gamma_3 = \pi/2$ and $\gamma_2 = \gamma_4 = 0$, we obtain

$$\frac{d}{dT_1}\theta_3 = \frac{d}{dT_1}\theta_4 = \frac{d}{dT_1}\theta_5 = \frac{d}{dT_1}\theta_6 \tag{26}$$

$$A_4 = A_3,\ A_{5..6} = -A_3 \tag{27}$$

$$A_1 = (-0.008152\sigma\, A_3 \pm 0.008152\sqrt{\sigma^2 + 4624.0})\, A_3 \tag{28}$$

It can be seen that Eq. (27) presents the correlation between the blade lead–lag oscillations and that Eq. (28) highlights the interconnection between the fuselage and blade amplitudes. Fig. 5 illustrates the two possible solutions at equilibrium (according to the sign "+" or "−" present in the equation) by plotting the evolution of A_1/A_3 as a function of the detuning parameter σ.

Now, regarding phase expressions, $\theta_3(T_1)$ is found by substituting Eq. (28) and γ_n values in Eq. (23). The remainders θ_n are obtained later from Eq. (24), except for θ_2 which is obtained directly from Eq. (23).

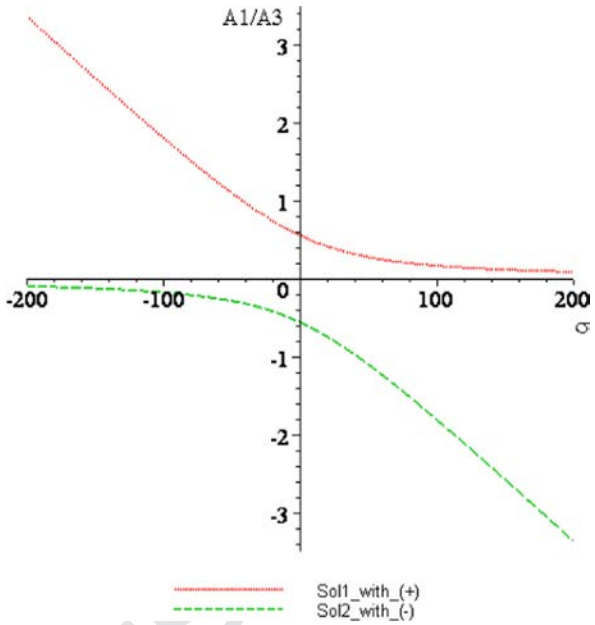

Fig. 5. Evolution of the ratio between the longitudinal amplitude of the fuselage and the in-plane blade rotation as a function of σ for case A.

$$\theta_1 = -\frac{\pi}{2} + \Theta_3 + 0.5000\sigma T_1 \pm 0.5000 T_1\sqrt{\sigma^2 + 4624.0}$$
$$\theta_2 = \Theta_2$$
$$\theta_3 = \Theta_3 - 0.5000\sigma T_1 \pm 0.5000 T_1\sqrt{\sigma^2 + 4624.0}$$
$$\theta_4 = -\frac{\pi}{2} + \Theta_3 - 0.5000\sigma T_1 \pm 0.5000 T_1\sqrt{\sigma^2 + 4624.0}$$
$$\theta_5 = \Theta_3 - 0.5000\sigma T_1 \pm 0.5000 T_1\sqrt{\sigma^2 + 4624.0}$$
$$\theta_6 = -\frac{\pi}{2} + \Theta_3 - 0.5000\sigma T_1 \pm 0.5000 T_1\sqrt{\sigma^2 + 4624.0} \tag{29}$$

Constants Θ_2 and Θ_3 are established from the initial conditions. Due to the fact that Eq. (28) is composed of two expressions, θ_n has the same property and follows the same order of signs.

By considering Eqs. (21), (27) and (28) in the solutions of Eq. (8), and by not taking into account the responses of u_{n_1}, the dynamic response of the helicopter, defined in Eq. (7), becomes the following at equilibrium:

$$u_{1\pm}(t) = A_1 e^{i(\omega_1 t + \theta_1)}$$
$$u_{2\pm}(t) = A_2 e^{i(\omega_2 t + \theta_2)}$$
$$u_{n\pm}(t) = A_3 e^{i(\omega_3 t + \theta_n)}, \quad n = 3\ldots4$$
$$u_{n\pm}(t) = -A_3 e^{i(\omega_3 t + \theta_n)}, \quad n = 5\ldots6 \tag{30}$$

The $u_{n\pm}$ consists of two different expressions depending on the sign used in Eq. (29) which also refers to the sign used in Eq. (28).

Assuming that at initial time $A_2 = \Theta_2 = 0$, $A_3 = 0.1$ and $\Theta_3 = \pi/2$ in Eq. (30), Figs. 6 and 7 illustrate the responses u_{n+} and u_{n-} of the helicopter, respectively, as a function of the azimuth angle of the first blade ψ_1 for $\sigma = [-25, 25]$. Appendix A illustrates the numerical expressions of the responses as a function of time.

A constant amplitude of 0.1 *rad* is verified for the blade lead–lag oscillations as is a null lateral displacement of the fuselage. Also, a decrease in amplitude of the longitudinal movement of the fuselage is also observed from case (a) to (b) in the responses u_{n+}, whereas the amplitude increases in responses u_{n-}. This conforms to the solutions given by A_1/A_3 along with σ, as shown in Fig. 5.

However, when regarding u_{n+} and u_{n-} for all cases of σ, it can be seen that A_3 and A_4 is phase shifted by 180° when compared to A_5 and A_6, respectively, while A_3 has a 90° phase shift related to A_6.

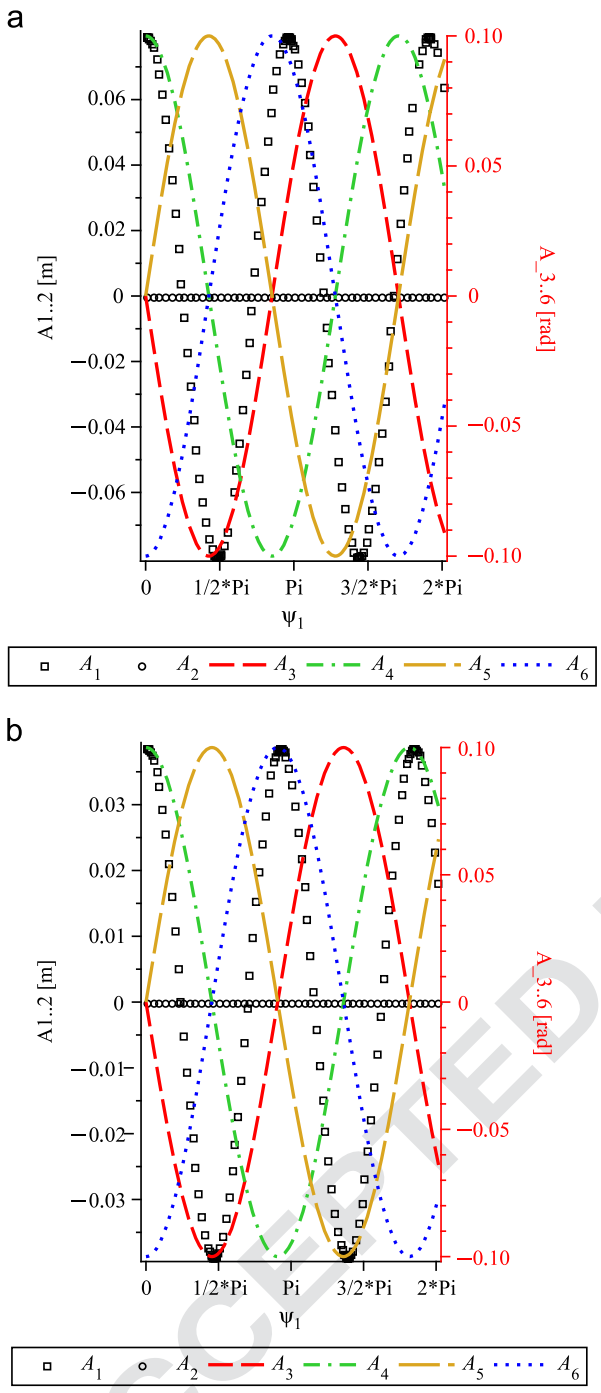

Fig. 6. Amplitude responses u_{n+} of the helicopter for the resonance case A along with azimuth angle of the first blade ψ_1. (a) $\sigma=-25$ and (b) $\sigma=25$.

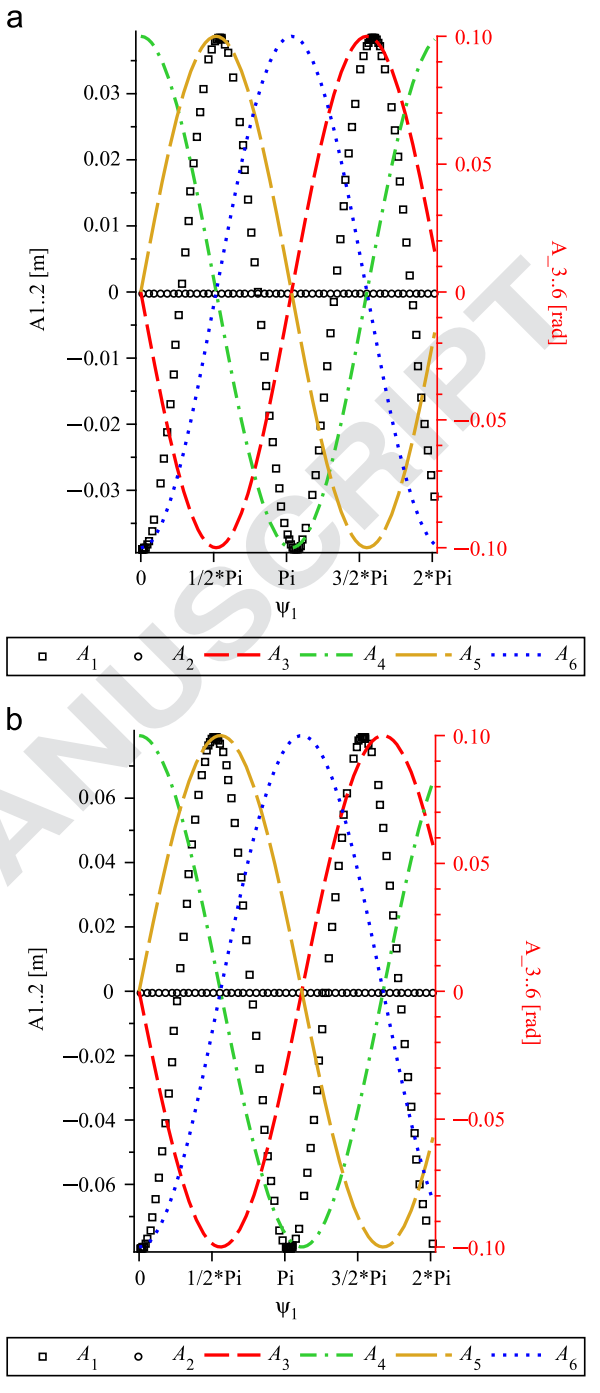

Fig. 7. Amplitude responses u_{n-} of the helicopter for the resonance case A as a function of the azimuth angle of the first blade ψ_1. (a) $\sigma=-25$ and (b) $\sigma=25$.

When comparing the above results with the temporal responses of a helicopter obtained by step-by-step integration, there are obviously significant similarities when considering the equilibrium, level of amplitudes and phase shift in all cases for responses u_{n+} and u_{n-}. Nevertheless, the absence of a beat phenomenon on the predicted responses is due to the fact that the responses of order ϵ^1 equations are not taken into account. In Appendix 5.2.1 detailed information is given on the integration method and initial conditions.

A phase shift of 180° can be seen in the correlation between the longitudinal movement of the fuselage and the displacement of the center of mass of the rotor in responses u_{n+} and u_{n-}. In the equilibrium responses u_{n+}, the fuselage moves forward while the center of mass of the rotor moves rearward and vice-versa. However, in u_{n-}, the center of the mass oscillates in phase with the fuselage. Fig. 8 illustrates the phase shift by representing the deformation shapes from the equilibrium responses at the maximum elongation of the longitudinal displacement. Symbol "0" (zero) indicates the point at rest and the dotted lines represent zero level of the in-plane lead–lag angles.

The same procedure is used to establish the amplitude response analysis for the entire set of γ_n solutions presented in Eq. (25). Even when changing the phase shift values, they all cause the helicopter to have the same two deformation shapes at equilibrium.

Both equilibrium solutions shift the position of the center of mass as a function of the rotor's rotation axis. Also, a phase shift of

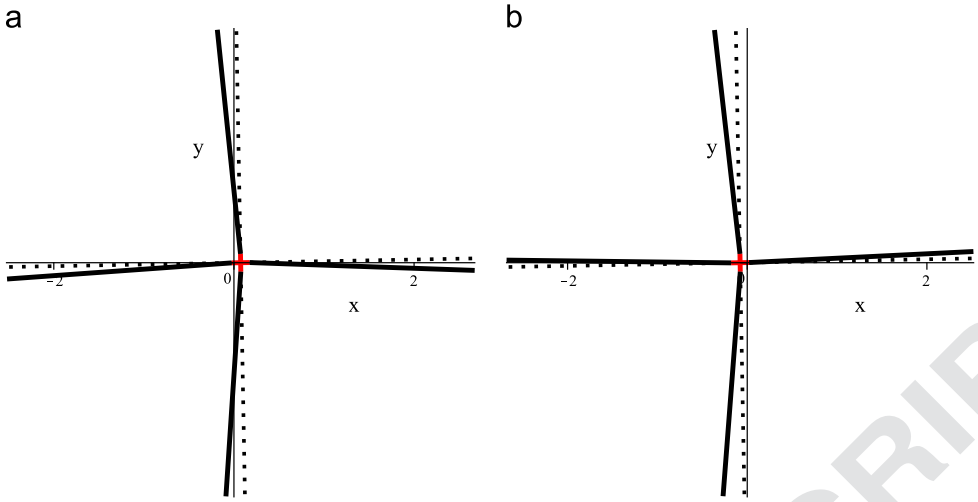

Fig. 8. Deformation shape of the helicopter in the resonance case A. (a) u_{n+} with $\sigma=-25$ and (b) u_{n-} with $\sigma=25$.

180° is detected between them when analyzing the longitudinal oscillation of the fuselage and the movement of the center of mass of the rotor.

5.2.2. Resonance case B

Similar to the previous study, the same series of actions is performed in order to complete the amplitude response analysis for resonance case B.

Once the polar transformation described in Eq. (21) is applied and the equations grouped it can be seen that the first equation of each set of equations is independent and null. The reason for this is linked to the non-existence of any harmonic terms at the same natural frequency for the longitudinal displacement of the fuselage (ω_1).

The list of expressions adopted for γ_n is as follows:

$$\gamma_n(T_1) = -\theta_2(T_1)+\sigma T_1+\theta_{n+2}(T_1), \quad n=1\ldots4 \tag{31}$$

Assuming the helicopter oscillates at equilibrium, the possible values for γ_n that satisfy the equations are

$$\begin{aligned}
&\gamma_1(T_1) = \{0,\pi\}\\
&\gamma_2(T_1) = \left\{\frac{\pi}{2},\frac{3\pi}{2}\right\}\\
&\gamma_3(T_1) = \{0,\pi\}\\
&\gamma_4(T_1) = \left\{\frac{\pi}{2},\frac{3\pi}{2}\right\}
\end{aligned} \tag{32}$$

Combining them leads to a set of sixteen γ solutions. The relation between the lateral displacement of the fuselage (A_2) as a function of the blade amplitudes (A_3–A_6) and the detuning parameters are determined for each one. The relation between blade amplitudes and phases are also predicted.

For example, taking into account one set of γ solutions, defined by $\gamma_1=\gamma_3=0$ and $\gamma_2=\gamma_4=\pi/2$, we obtain

$$\frac{d}{dT_1}\theta_3 = \frac{d}{dT_1}\theta_4 = \frac{d}{dT_1}\theta_5 = \frac{d}{dT_1}\theta_6 \tag{33}$$

$$A_{4\ldots5} = -A_3, \quad A_6 = A_3 \tag{34}$$

$$A_2 = (0.004713\sigma \pm 0.0001885\sqrt{625.0\sigma^2+6666000.0})\,A_3 \tag{35}$$

Note that two possible solutions express the relation between the lateral amplitude of the fuselage and the amplitude of the blade oscillations. Fig. 9 shows the evolution of the ratio of amplitudes A_2/A_3 with the detuning parameter σ.

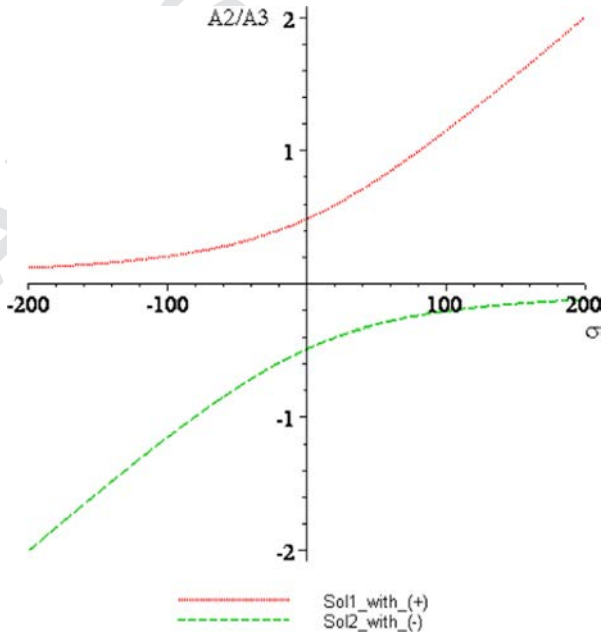

Fig. 9. Evolution of the ratio between the longitudinal amplitude of the fuselage and the in-plane blade rotation with σ for case B.

By replacing Eqs. (34) and (35) in the set of equations with real and imaginary terms, as in the previous study in case A, the expressions of θ_n are obtained as shown below:

$$\begin{aligned}
\theta_1 &= \Theta_1\\
\theta_2 &= \Theta_3+0.50000\sigma T_1 \mp 0.02000T_1\sqrt{625.0\sigma^2+6666000.0}\\
\theta_3 &= \Theta_3-0.50000\sigma T_1 \mp 0.02000T_1\sqrt{625.0\sigma^2+6666000.0}\\
\theta_4 &= \frac{\pi}{2}+\Theta_3-0.50000\sigma T_1 \mp 0.02000T_1\sqrt{625.0\sigma^2+6666000.0}\\
\theta_5 &= \Theta_3-0.50000\sigma T_1 \mp 0.02000T_1\sqrt{625.0\sigma^2+6666000.0}\\
\theta_6 &= \frac{\pi}{2}+\Theta_3-0.50000\sigma T_1 \mp 0.02000T_1\sqrt{625.0\sigma^2+6666000.0}
\end{aligned} \tag{36}$$

Constants Θ_1 and Θ_3 are defined through the initial conditions. By respecting the order in which the expressions are obtained, sign "$\mp$" appears. This means that an expression containing "+" in Eq. (35) leads to sign "−" in Eq. (36). Unlike the previous study

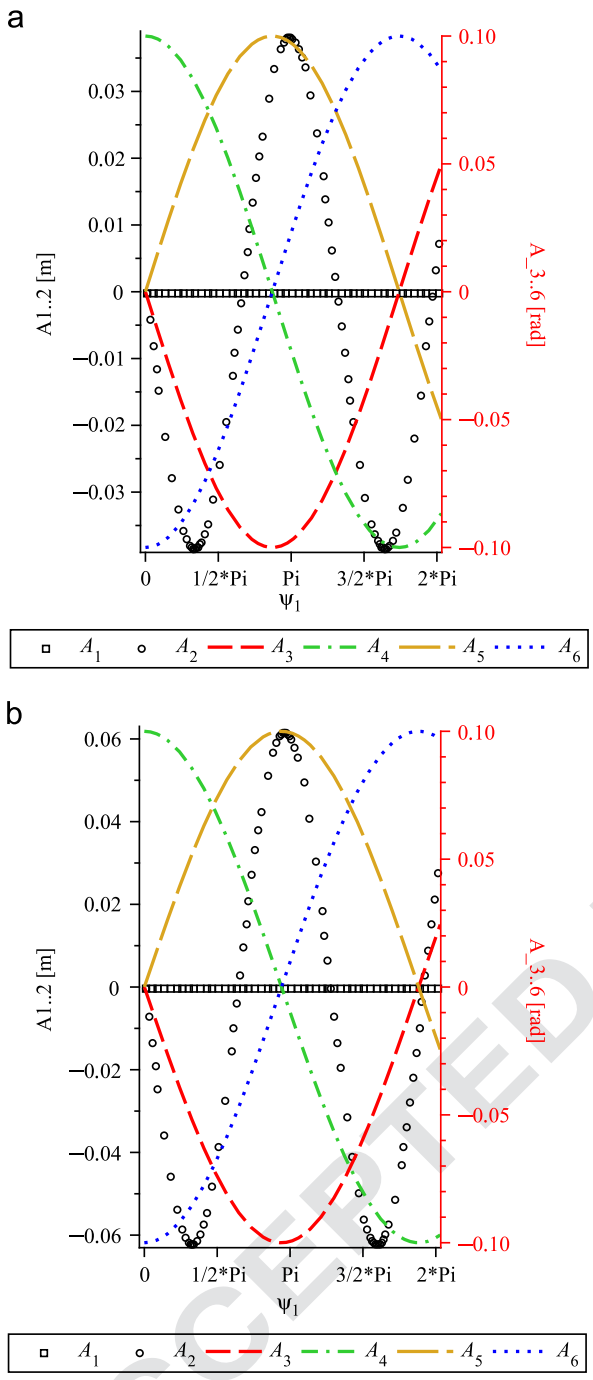

Fig. 10. Amplitude responses u_{n+} of the helicopter for the resonance case B along with azimuth angle of the first blade ψ_1. (a) $\sigma = -25$ and (b) $\sigma = 25$.

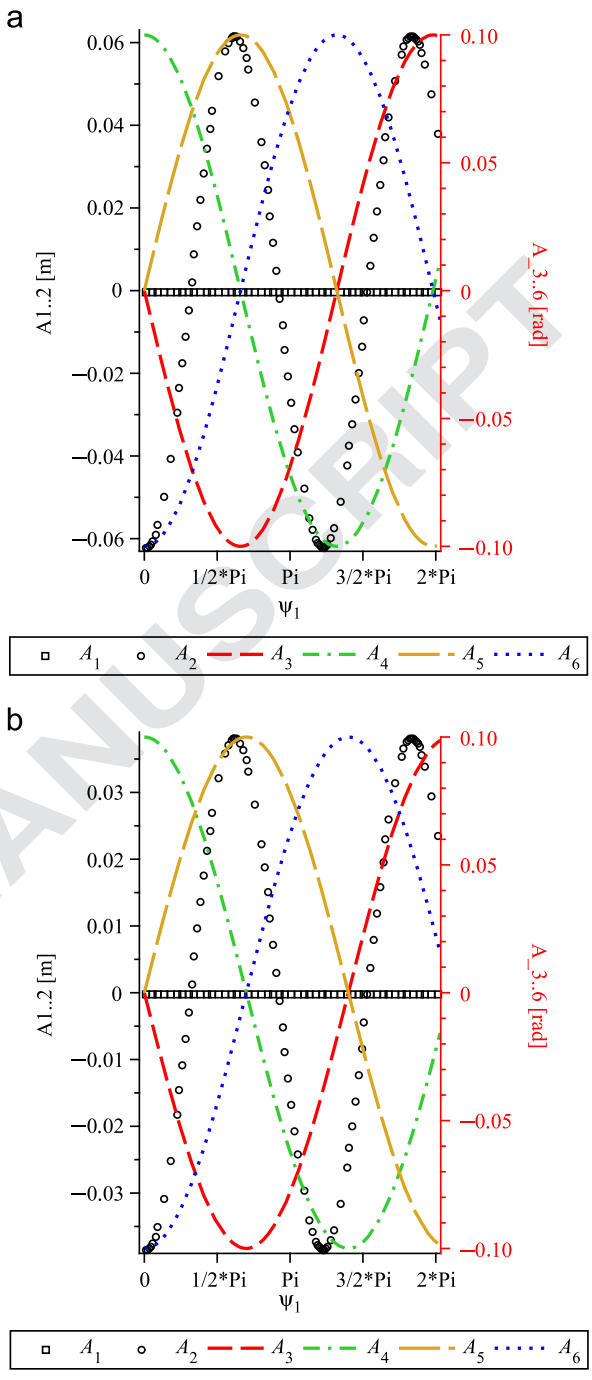

Fig. 11. Amplitude responses u_{n-} of the helicopter for the resonance case B as a function of the azimuth angle of the first blade ψ_1. (a) $\sigma = -25$ and (b) $\sigma = 25$.

of resonance case A, the solution with sign "+" increases as σ increases.

Finally, knowing the relation between the phase and amplitudes of each degree of freedom, the expressions for the responses at equilibrium u_{n+} and u_{n-} of the helicopter are determined.

By imposing $A_1 = \Theta_1 = 0$, $A_3 = 0.1$ and $\Theta_3 = \pi/2$ as initial conditions (see the appendix where their numerical expressions are given as a function of time Appendix A). Figs. 10 and 11 illustrate the amplitude responses of the helicopter as a function of the azimuth angle of the first blade ψ_1 for $\sigma = [-25,\ 25]$.

By comparing the results obtained for resonance cases A and B, it is possible to verify the same characteristics regarding the phase shift between the blade movements. However, regarding the level of amplitude of the oscillations, the blades reaches 0.1 rad, while the lateral displacement attains 0.06 m and the longitudinal movement is null. The first and third statements (blade and longitudinal movement) are consequences of the initial conditions while the second obeys the ratio A_2/A_3 as a function of σ shown in Fig. 9.

Taking the previous resonance case into account, a comparison of the results with the temporal responses of a helicopter achieved by step-by-step integration (see Appendix 5.2.1) highlights significant similarities when the equilibrium, level of amplitudes and phase shift in all cases for responses u_{n+} and u_{n-} is examined. Nevertheless, the absence of a beat phenomenon on the predicted responses is due to the fact that the responses of order ϵ^1 equations are not taken into account.

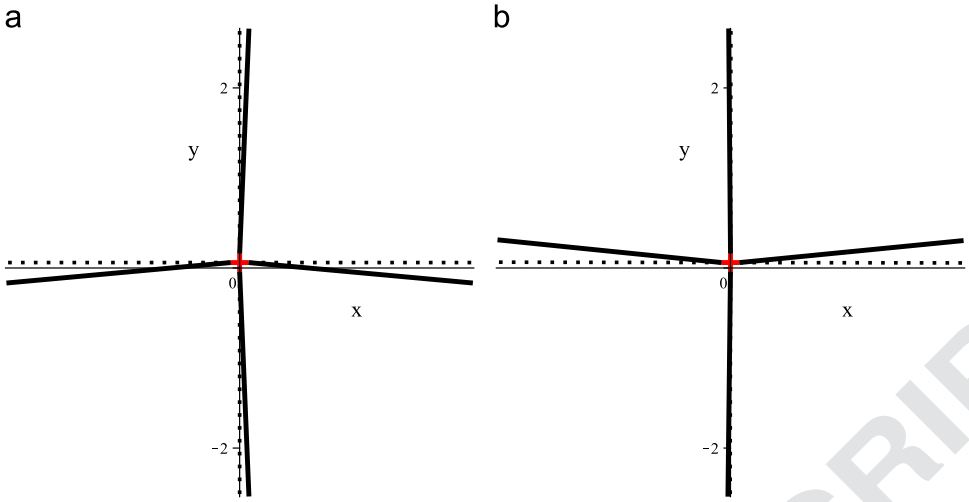

Fig. 12. Deformation shape of the helicopter in the resonance case B. (a) u_{n-} with $\sigma=-25$ and (b) u_{n+} with $\sigma=25$.

In the correlation between the lateral movement of the fuselage and the displacement of the center of mass of the rotor in responses u_{n+} and u_{n-}, a phase shift of 180° can be observed when comparing these two equilibrium solutions. Fig. 12 illustrates the phase shift by representing the deformation shapes. Symbol "0" (zero) indicates the rest point and the dotted lines represent the zero level of the in-plane lead-lag angles.

The procedure developed is repeated in order to achieve the amplitude response analysis for the whole set of γ_n solutions presented in Eq. (32) for resonance case B.

The results verify the same shape deformation for the whole set of γ_n solutions and there is a phase shift of 180° between the lateral movement of the fuselage and the blade oscillations when comparing the equilibrium responses at resonance case B. Both shift the center of mass of the rotor from the axis of rotation.

6. Conclusion

In recent decades the ground resonance phenomenon has attracted much attention from researchers. Predicting the critical rotor speeds at which the phenomenon occurs requires carrying out a stability analysis on the periodical equations of motions.

The aim of this paper consisted in considering the helicopter as a parametrically excited system and using the Method of Multiple Scales. The reasons for this are mainly due to the advantages of using methods that give analytical responses (e.g., versatility and CPU time) and that determine the existence of parametric resonances. Stability analysis on each of these resonances leads to identifying the instability regions and their boundaries. Moreover, a study of the amplitude response was carried out in stable resonant cases.

A numerical analysis was carried out for one aircraft configuration with an isotropic rotor. Four parametric resonant cases (cases A, B, C and D) were detected with first order equations. The order terms higher than $\mathcal{O}(2)$ were neglected in the expansion development with MMS. Instability regions were detected in cases C and D, and they were linked to the existence of unstable parametric resonances. They were expressed as a combination of the natural frequencies of the blades and fuselage. The boundaries of instability established with MMS were compared and validated with those obtained by using Floquet's Theory to a great degree of precision.

Nevertheless, the study of the amplitude responses of the helicopter for resonance cases A and B validates the presence of resonant points. In both cases, two solutions were found for resonance cases A and B at which the dynamical system is in equilibrium. This was achieved by not considering the responses of ϵ^1 equations and by imposing a constant in-plane lead lag oscillation of the blades. Regarding the motion of the center of mass of the rotor and by comparing the fuselage movement between these solutions, a phase shift of 180° was detected. Both cases A and B led to a shift of the center of mass from the rotation axis of the rotor.

Appendix A. Numerical responses expressions

In this appendix, the numerical expressions at equilibrium u_{n+} and u_{n-} are determined for both resonance cases A and B. The expressions of u_{n+} and u_{n-} are determined for both resonance cases A and B.

- Resonance case A:

Once the numerical values of the initial conditions described in Section 5.2.1 have been substituted in Eq. (30) and by respecting the value admitted for σ, the expressions of u_{n+} are

$$\sigma=-25\rightarrow\begin{cases}u_{1+}=0.079454\cos(19.473t)\\ u_{2+}=0.\\ u_{3+}=0.10000\cos(10.863t+1.5708)\\ u_{4+}=0.10000\cos(10.863t)\\ u_{5+}=-0.10000\cos(10.863t+1.5708)\\ u_{6+}=-0.10000\cos(10.863t)\end{cases}\tag{A.1}$$

$$\sigma=25\rightarrow\begin{cases}u_{1+}=0.038686\cos(20.131t)\\ u_{2+}=0.\\ u_{3+}=0.10000\cos(10.206t+1.5708)\\ u_{4+}=0.10000\cos(10.206t)\\ u_{5+}=-0.10000\cos(10.206t+1.5708)\\ u_{6+}=-0.10000\cos(10.206t)\end{cases}\tag{A.2}$$

whereas the expressions of u_{n-} are

$$\sigma=-25\rightarrow\begin{cases}u_{1-}=-0.038686\cos(17.568t)\\ u_{2-}=0.\\ u_{3-}=0.10000\cos(8.9581t+1.5708)\\ u_{4-}=0.10000\cos(8.9581t)\\ u_{5-}=-0.10000\cos(8.9581t+1.5708)\\ u_{6-}=-0.10000\cos(8.9581t)\end{cases}\tag{A.3}$$

$$\sigma = 25 \rightarrow \begin{cases} u_{1-} = -0.079454\ \cos(18.226t) \\ u_{2-} = 0. \\ u_{3-} = 0.10000\ \cos(8.3006t + 1.5708) \\ u_{4-} = 0.10000\ \cos(8.3006t) \\ u_{5-} = -0.10000\ \cos(8.3006t + 1.5708) \\ u_{6-} = -0.10000\ \cos(8.3006t) \end{cases} \quad (A.4)$$

- Resonance case B:

Once the numerical values of the initial conditions described in section 5.2.2 have been substituted in Eq. (30) and by respecting the value admitted for σ, the expressions of u_{n+} are

$$\sigma = -25 \rightarrow \begin{cases} u_{1+} = 0. \\ u_{2+} = 0.038296\ \cos(23.407t + 1.5708) \\ u_{3+} = 0.10000\ \cos(1.5708 + 8.7782t) \\ u_{4+} = -0.10000\ \cos(3.1416 + 8.7782t) \\ u_{5+} = -0.10000\ \cos(1.5708 + 8.7782t) \\ u_{6+} = 0.10000\ \cos(3.1416 + 8.7782t) \end{cases} \quad (A.5)$$

$$\sigma = 25 \rightarrow \begin{cases} u_{1+} = 0. \\ u_{2+} = 0.061861\ \cos(24.064t + 1.5708) \\ u_{3+} = 0.10000\ \cos(1.5708 + 8.1207t) \\ u_{4+} = -0.10000\ \cos(3.1416 + 8.1207t) \\ u_{5+} = -0.10000\ \cos(1.5708 + 8.1207t) \\ u_{6+} = 0.10000\ \cos(3.1416 + 8.1207t) \end{cases} \quad (A.6)$$

whereas the expressions of u_{n-} are

$$\sigma = -25 \rightarrow \begin{cases} u_{1-} = 0. \\ u_{2-} = -0.061861\ \cos(26.201t + 1.5708) \\ u_{3-} = 0.10000\ \cos(1.5708 + 11.573t) \\ u_{4-} = -0.10000\ \cos(3.1416 + 11.573t) \\ u_{5-} = -0.10000\ \cos(1.5708 + 11.573t) \\ u_{6-} = 0.10000\ \cos(3.1416 + 11.573t) \end{cases} \quad (A.7)$$

$$\sigma = 25 \rightarrow \begin{cases} u_{1-} = 0. \\ u_{2-} = -0.038296\ \cos(26.859t + 1.5708) \\ u_{3-} = 0.10000\ \cos(1.5708 + 10.915t) \\ u_{4-} = -0.10000\ \cos(3.1416 + 10.915t) \\ u_{5-} = -0.10000\ \cos(1.5708 + 10.915t) \\ u_{6-} = 0.10000\ \cos(3.1416 + 10.915t) \end{cases} \quad (A.8)$$

Appendix B. Temporal responses

Figs. B1–B4 illustrate the temporal responses of a helicopter for resonance cases A and B. The results were obtained from a step-by-step numerical integration Adams113 with Matlab®. The initial conditions of position and speed are determining from the equilibrium solutions in Eqs. (A.1)–(A.4) for case A and from Eqs. (A.5)–(A.8) for case B.

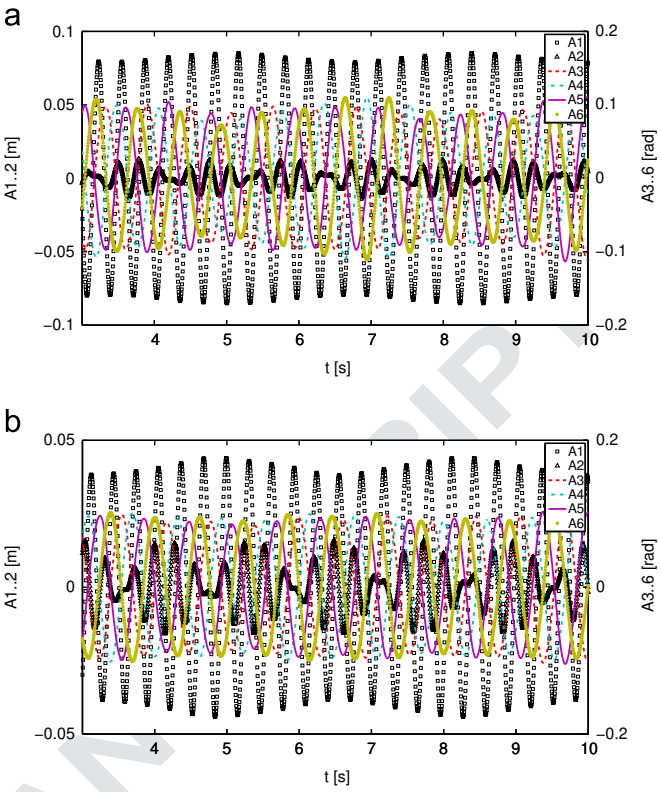

Fig. B1. Time response of helicopter in resonance case A by respecting the initial conditions of responses u_{n+}. (a) $\sigma = -25$ and (b) $\sigma = 25$.

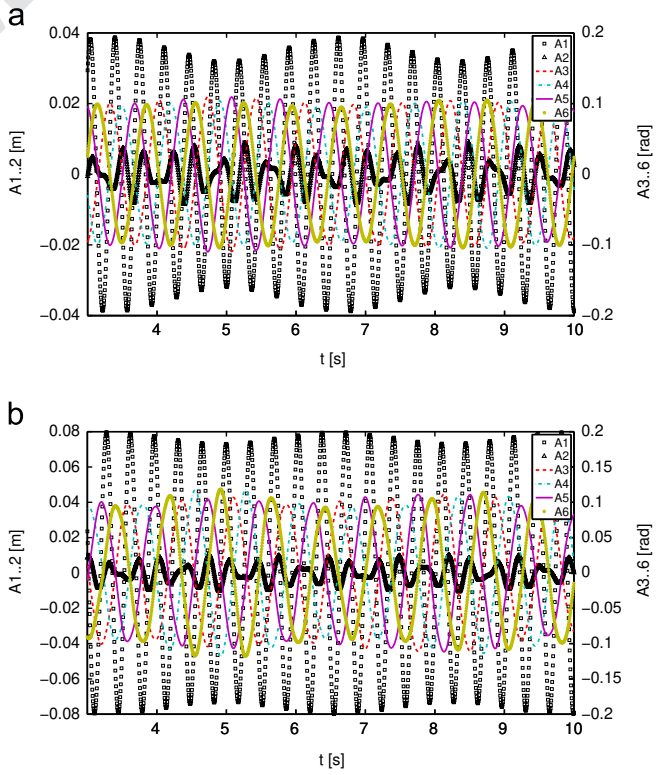

Fig. B2. Time response of helicopter in resonance case A by respecting the initial conditions of responses u_{n-}. (a) $\sigma = -25$ and (b) $\sigma = 25$.

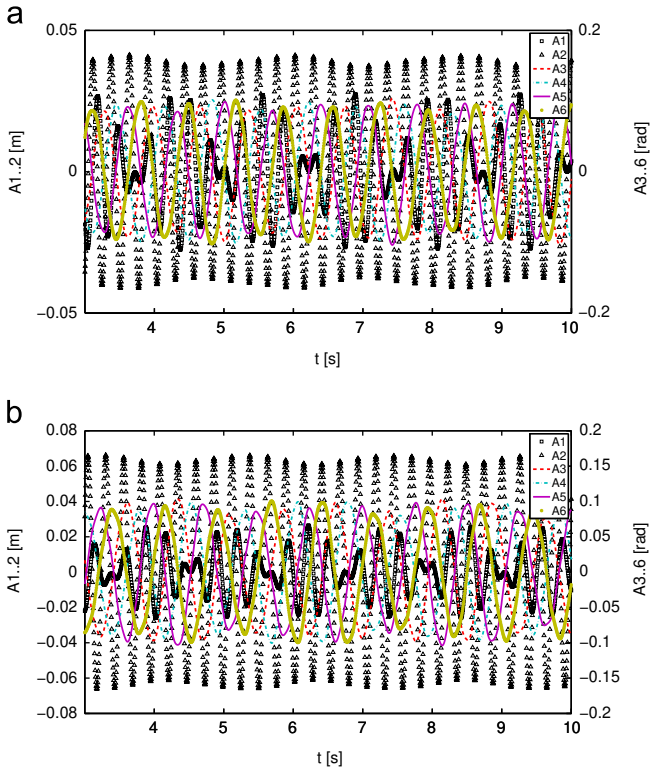

Fig. B3. Time response of a helicopter in resonance case B by conforming to the initial conditions of responses u_{n+}. (a) $\sigma=-25$ and (b) $\sigma=25$.

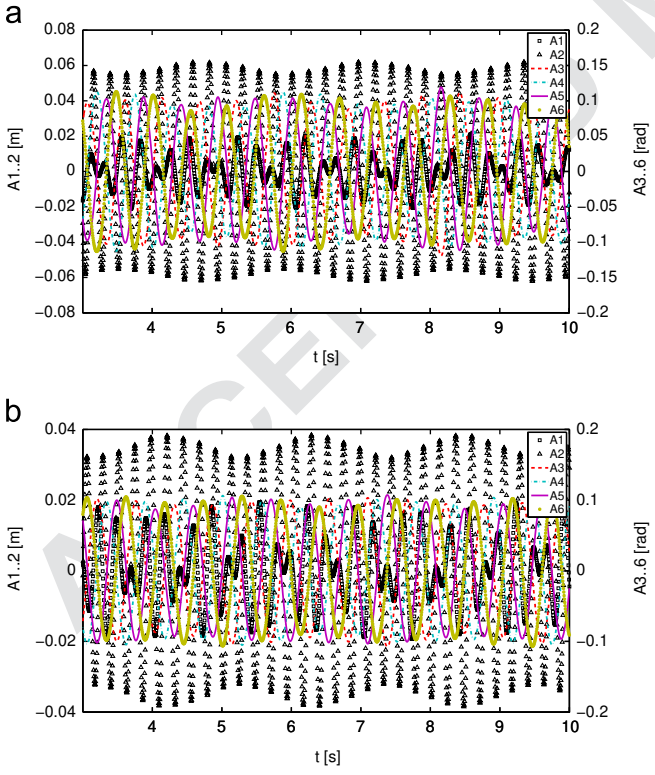

Fig. B4. Time response of a helicopter in resonance case B by conforming to the initial conditions of responses u_{n-}. (a) $\sigma=-25$ and (b) $\sigma=25$.

References

[1] R. Ganiev, I. Pavlov, The theory of ground resonance of helicopters, Int. Appl. Mech. 9 (1973) 505–510.

[2] R. Coleman, A. Feingold, Theory of Self-Excited Mechanical Oscillations of Helicopter Rotors with Hinged Blades, Technical Report, Report no. 1351, NACA Techinical Note 3844, 1957.

[3] R. Donham, S. Cardinale, I. Sachs, Ground and air resonance characteristics of a soft in-plane rigid-rotor system, J. Am. Helicopter Soc. 14 (1969) 33.

[4] R. Lytwyn, W. Miao, W. Woitsch, Airborne and ground resonance of hingeless rotors, J. Am. Helicopter Soc. 16 (1971) 2.

[5] D. Hodges, An aeromechanical stability analysis for bearingless rotor helicopters, J. Am. Helicopter Soc. 24 (1979) 02.

[6] D. Kunz, Nonlinear analysis of helicopter ground resonance, Nonlinear Anal.: Real World Appl. 3 (3) (2002) 383–395.

[7] L. Byers, F. Gandhi, Embedded absorbers for helicopter rotor lag damping, J. Sound Vib. 325 (4–5) (2009) 705–721.

[8] G. Bir, Multi-blade coordinate transformation and its application to wind turbine analysis, in: Proceedings of AIAA/ASME Wind Energy Symposium, 2008.

[9] L. Sanches, G. Michon, A. Berlioz, D. Alazard, Modélisation Dynamique d'un Rotor sur Base Flexible (Dynamic Modeling of a Rotor Over a Flexible Base), in: Congress Français de Mécanique, 24–28 August, Marseille, 2009.

[10] L. Sanches, G. Michon, A. Berlioz, D. Alazard, Instability zones for isotropic and anisotropic multibladed rotor configurations, Mech. Mach. Theory 46 (8) (2011) 1054–1065, ISSN 0094-114X, http://dx.doi.org/10.1016/j.mechmachtheory.2011.04.005.

[11] C. Hammond, An application of Floquet theory to prediction of mechanical instability, J. Am. Helicopter Soc. 19 (1974) 14.

[12] A. Nayfeh, D. Mook, Nonlinear Oscillations, John Wiley & Sons Incorp., New York, 1979.

[13] A. Nayfeh, Perturbation Methods, Wiley-VCH Verlag GmbH & CO. KGaA, Germany, 2004.

[14] G. Michon, L. Manin, R. Parker, R. Dufour, Duffing oscillator with parametric excitation: analytical and experimental investigation on a belt-pulley system, J. Comput. Nonlinear Dyn. 3 (2008) 031001.

[15] M.R. Shad, G. Michon, A. Berlioz, Modeling and analysis of nonlinear rotordynamics due to higher order deformations in bending, Appl. Math. Model. 35 (5) (2011) 2145–2159.

[16] N. Driot, C. Lamarque, A. Berlioz, Theoretical and experimental analysis of a base-excited rotor, J. Comput. Nonlinear Dyn. 1 (2006) 257.

[17] M. Duchemin, A. Berlioz, G. Ferraris, Dynamic behavior and stability of a rotor under base excitation, J. Vib. Acoust. 128 (2006) 576.

[18] X. Xu, M. Wiercigroch, Approximate analytical solutions for oscillatory and rotational motion of a parametric pendulum, Nonlinear Dyn. 47 (1) (2007) 311–320.

[19] R. Dufour, A. Berlioz, Parametric instability of a beam due to axial excitations and to boundary conditions, J. Vib. Acoust. 120 (2) (1998) 461–467.